NASA Technical Memorandum 103218

Unsteady Blade-Surface Pressures on a Large-Scale Advanced Propeller: Prediction and Data

M. Nallasamy
Sverdrup Technology, Inc.
Lewis Research Center Group
Brook Park, Ohio

and

J.F. Groeneweg
National Aeronautics and Space Administration
Lewis Research Center
Cleveland, Ohio

NASA

UNSTEADY BLADE-SURFACE PRESSURES ON A LARGE-SCALE ADVANCED PROPELLER: PREDICTION AND DATA

M. Nallasamy
Sverdrup Technology, Inc.
Lewis Research Center Group
Brook Park, Ohio 44142

and

J.F. Groeneweg
National Aeronautics and Space Administration
Lewis Research Center
Cleveland, Ohio 44135

Summary

An unsteady, three-dimensional Euler analysis technique was used to compute the flowfield of an advanced propeller operating at an angle of attack. The predicted blade-pressure waveforms for an angular inflow of 3° were compared with wind tunnel data at two Mach numbers, 0.5 and 0.2. For an inflow Mach number of 0.5, the predicted pressure response is in fair agreement with data: the predicted phases of the waveforms are in close agreement with data, whereas the magnitudes are underpredicted. At the low Mach number of 0.2 (takeoff), the numerical solution shows the formation of a leading-edge vortex which is in qualitative agreement with measurements. However, the highly nonlinear pressure response measured on the blade suction surface is not captured in the present inviscid analysis.

Introduction

Advanced propellers are highly loaded, variable pitch turboprops designed to operate at high speeds and to achieve a higher propulsive efficiency than is achieved by the current high-bypass turbofans. The thin, highly swept blades of these propellers can produce a complex flowfield with leading edge vortices, tip vortices, and/or shock waves, depending on the operating conditions. Detailed measurements of the blade-surface steady (ref. 1) and unsteady (ref. 2) pressures have been carried out to understand the nature of the propfan flows. These tests were carried out on a large-scale 9-ft-diameter single-rotation, SR7L propeller

in a transonic wind tunnel in Modane, France. The propeller was operated in a two-bladed configuration (fig. 1) because there was not enough power to run the eight-bladed design propeller.

The blade surface pressure was measured on a specially designed, pressure-tapped SR7L blade. Unsteady blade-surface pressure data were obtained for propfan operation with a 3° angular inflow and a wake inflow, over a range of Mach numbers from 0.02 to 0.7 (ref. 2). These pressures were measured at two radial stations (fig. 2) with pressure transducers on both suction and pressure sides. At the inboard station (r/R = 0.641, where r is the radial distance to the point and R is the blade tip radius), there were seven pressure transducers on each side of the blade, while at the outboard station (r/R = 0.906), there were six on each side. Tests were conducted at static propeller conditions, take-off conditions, and different power-loading conditions at Mach 0.5 (including one at the design-cruise power loading, on a per-blade basis).

Comparisons of Euler solutions and Modane wind tunnel test data for steady flow (0° inflow angle) conditions were made over a range of Mach numbers by Nallasamy et al. (ref. 3). The present investigation evaluates the ability of an unsteady Euler analysis technique to predict the unsteady pressure distribution on a propfan with angular inflow. It compares the predicted pressure-time histories for an angular inflow of 3° with the Modane wind-tunnel test data for two inflow Mach numbers, 0.5 and 0.2.

Numerical Solution of Unsteady, Three-Dimensional Euler Equations

The unsteady, three-dimensional Euler equations governing the inviscid flow through a propeller are solved employing a solution procedure developed by Whitfield et al. (refs. 4 and 5). In this procedure, the Euler equations in conservative, differential form are transformed from a Cartesian reference frame to a body-fitted, curvilinear reference frame. Then the transformed equations are discretized employing a finite volume technique. An approximate Riemann solver is used for block interface flux definitions, and a lower-upper (LU) implicit numerical scheme is used to solve the discretized equations. (Further details of the solution procedure may be found in refs. 4 and 5.) The flowfield is represented by multiblock composite grids to limit the core memory requirements. When the solution at each time step is updated, only one block is stored in the core memory while other blocks are stored on solid-state storage devices (SSD). The authors also used this solution procedure to compute the unsteady flowfield of an eight-bladed SR7L propeller with angular inflow at cruise conditions (Mach 0.8) (refs. 6 and 7). The present computations were carried out on the Cray Y-MP computer at NASA Ames Research Center. With the time step and grid resolution employed in this study, a complete run for one test condition took about 33 CPU hr.

Computational Grid

The configuration considered is that of the two-bladed, SR7L Modane test, which is shown in figure 1 along with the direction of rotation and the axes of reference. In the computations, azimuth angle ϕ was measured from the z axis, as shown. This azimuth angle (ϕ) reference is used only in figure 4; in all other figures $\phi = 0$ corresponds to top-dead-center, as in the presentation of experimental results in reference 2. An H-grid is employed to represent the flowfield. This grid was generated by a special purpose mesh generator developed for propfans (ref. 8).

Each of the two blade passages is described by 107 by 41 by 45 (axial by radial by circumferential) grid points, and each passage grid is divided into 11 blocks (107 by 41 by 5

grid points in each) for computational convenience, as mentioned earlier. Thus 22 blocks of grid describe the entire flowfield (two-blade passages) with 394 830 nodal points. Each blade surface is represented by 49 by 27 (chordwise by spanwise) grid points with higher resolution near the leading and trailing edges, the hub, and the tip. In figure 3, parts (a) to (c) show the bladewise surface, streamwise surface, and spanwise surface views of the grid, respectively. Figure 3(d) shows the distribution of grid points on the blade surface and around it. The far-field boundary is three blade radii from the blade tip, the inflow plane is two blade radii upstream of the spinner, and the exit plane is two blade radii behind the blade. These boundary locations have been found to be adequate for angular inflow computations (refs. 6 and 7).

Results and Discussion

Two representative unsteady test cases with 3° angular inflow were chosen for detailed comparison of the predictions and experimental data. The test operating conditions are shown in table I. For test 8, the advance ratio and power coefficient, on a per-blade basis, were nearly equal to the cruise values, so the nondimensional loading and flow angles were approximately preserved. Test 6 represents high-power takeoff for which the measured steady pressure distributions indicate the presence of a leading edge vortex (ref. 1).

The unsteady Euler solutions were obtained for these two tests with the grids generated using the nominal blade setting angles at 75-percent radius ($\beta_{3/4}$) of the experiments (table I). No attempt was made to match exactly the measured and predicted total power coefficients. The solutions were carried out from an impulse start for three complete revolutions of the propeller to obtain a reasonably accurate solution. The results of the third revolution are stabilized as indicated by a periodic variation of per-blade power coefficient (fig. 4) during the second and third revolutions of the propeller. Running the solution through the fourth revolution produced no recognizable change in the variables of interest. The results of the third revolution are analyzed, and pressure waveforms are compared with the experimental data.

TABLE I. - OPERATING CONDITIONS FOR UNSTEADY BLADE-SURFACE
PRESSURE MEASUREMENTS

Modane test	Mach number, M	Advance ratio, J	Blade speed, rpm	Blade setting angle at 75-percent radius, $\beta_{3/4}$, deg
6	0.2	0.881	1671	31.6
8	.5	3.062	1193	55.5

2

The pressure coefficient is defined in this paper as

$$Cp = \sum_{ij} \frac{P_{ij} - P_\infty}{0.5\rho_\infty \left(V_\infty^2 + r_{ij}^2 \omega^2 \right)}$$

where P_{ij} and r_{ij} are the local pressure and radial distances of a point; P_∞, ρ_∞, and V_∞ are the pressure, density, and velocity of the free stream, respectively, and ω is the rotational speed (rad/sec) of the blade. The instantaneous power coefficient per blade is computed from instantaneous blade surface pressures by

$$CP = \sum_{ij} \frac{2\pi}{\rho_\infty \Omega^2 D^5} r_{ij} \left(P_{ij} \, \Delta\vec{A}_{ij} \right)_\phi$$

where $\Delta\vec{A}_{ij}$ is the elemental surface area formed by four neighboring grid points, r_{ij} is the radial distance of the element, D is the diameter of the propeller, and Ω is the rotational velocity (rev/sec). The subscript ϕ denotes the component in the tangential direction.

The predicted total time-mean power coefficient of the propeller (for two blades) for test 8 (M = 0.5, J = 3.062) is 2 percent higher than the measured value of 0.361, whereas that for test 6 (M = 0.2, J = 0.881) is 5 percent higher than the measured value of 0.251. Figure 4 shows the variation of the single-blade power coefficient with azimuth angle for the two test cases considered. The blade starts at $\phi = 0$, and the variation of the power coefficient is shown for three revolutions of the blade. The expected sinusoidal variation of the blade loading due to angular inflow is clearly observed in both cases. The amplitude of the power coefficient varies ±65 percent of the mean for test 8 and ±9 percent of the mean for test 6.

A Fourier transform of the third-cycle blade power coefficient variation gives CP = a_0 - $a_i \cos \omega t$ - $b_i \sin \omega t$, where a_0, a_i, and b_i are the Fourier coefficients and t is the time. The loading spectra for tests 6 and 8 are shown in figure 5. The first harmonic dominates the loading, which lags the blade motion for tests 8 and 6 by angles of 10.5° and 17.5°, respectively.

The chordwise distributions of the steady blade-surface pressures computed for test 8 agree well with experimental data (ref. 3). Figure 6 shows the unsteady blade-surface pressure as a function of azimuth angle for the inboard radial station r/R = 0.641 on the pressure surface for test 8. For the pressure waveforms given in this paper, 0° corresponds to top-dead-center as in the presentation of experimental data (ref. 2). The measured sinusoidal response of the propeller operating at an angle of attack is qualitatively reproduced by

the computations. The phases of the predicted waveforms agree well with data, and the predicted levels of the unsteady pressure are lower than the experimental levels. The data show that the blade has the largest response slightly downstream (x/c = 0.1) of the leading edge and has progressively less response towards the trailing edge. In the predictions, the largest response occurs near the leading edge (x/c = 0.049), and the response reduces gradually towards the trailing edge. The discrepancy between measured and predicted maximum response locations may have resulted because the leading-edge blade geometry of the test is not reproduced exactly in the computations.

The pressure waveforms on the suction surface of the blade are shown in figure 7. The predicted response and agreement with data are similar to those on the pressure side, but both the predicted and measured largest responses occur near the leading edge (x/c = 0.049) on the suction surface. Note that the pressures on the suction surface are nearly 180° out of phase with those on the pressure surface. The magnitudes are underpredicted as on the pressure surface. The pressure-time histories at the outboard radial station (r/R = 0.906) are shown in figure 8 for the pressure surface and in figure 9 for the suction surface. The agreement of the predicted level and phase of the pressure signals at this outboard radial station is similar to that at the inboard station: the phases of the pressures are in close agreement with data, whereas the magnitudes are underpredicted.

Oilflow studies of surface streamlines of the propeller blade operating under takeoff conditions (with 0° inflow angle) show the formation of a leading edge vortex (refs. 9 and 10). The steady surface-pressure measurements for Modane test 6 indicate the formation of a leading edge vortex (ref. 1). A broad hump in the suction-side, chordwise pressure distribution at r/R = 0.906, seems to indicate that the vortex has rolled up. With the present grid resolution, the steady pressure distribution is predicted reasonably well (not shown). The broad hump on the suction side pressure distribution is also predicted well.

Figure 10 shows the predicted azimuthal variation of the chordwise pressure coefficient distribution at r/R = 0.9 for test 6 with an angular inflow of 3°. Apparently, the vortex (indicated by the broad hump near the leading edge on the suction-side pressure coefficient curve) stays on the blade for the entire revolution. The experimental data are also shown in the figure. For test 6, at this radial station, only three pressure transducers were operating on each surface (as for test 8). The agreement of the predicted pressure coefficients on the pressure surface with data is good at all four azimuthal locations. On the suction surface, the pressure coefficients are under-predicted. The discrepancy is greatest at the azimuthal location $\phi = 270°$. As discussed later, the pressure waveforms on the suction surface are dominated by nonlinear viscous effects which are not

3

represented by the present inviscid calculations. Also note that the data points in this figure were derived from the computed-time mean pressure at each transducer location. (The time-mean pressures of the experiment were not available.)

As indicated by figure 10, only slight changes in the size and strength of the vortex occur as the azimuthal location of the blade is varied. These changes are illustrated in figure 11. The figure shows the suction surface static pressure contours which indicate the presence of the vortex for the upward-moving blade (lightly loaded) and downward-moving blade (heavily loaded). In the present case, the closed contours distinguish the vortex from a low-pressure region produced by the flow expansion at the leading edge due to the high incidence angle. The variations of the size and strength of the vortex with azimuthal location of the blade are clearly shown although the magnitudes are small.

Numerical solutions of the Euler equations predict the leading edge vortices on swept wings and delta wings fairly well (refs. 11 and 12) although the mechanism responsible for the formation of the vortex in these calculations is not clear (refs. 13 and 14). However, the ability of the unsteady Euler solutions to predict the time dependence of the vortex as in the present case needs to be studied further and compared with data. Such detailed data defining the time dependence of the vortex are not currently available.

The pressure waveforms for test 6 with 3° angular inflow are shown in figure 12 for the pressure side at the inboard radial station (r/R = 0.641). The blade-pressure response is very low, and the predictions agree with the data. On the suction surface (fig. 13), the data show nonsinusoidal response at all transducer locations. Such a nonlinear response is not predicted by the Euler solution. At the outboard radial station (r/R = 0.906), the pressure waveforms on the pressure side (fig. 14) show sinusoidal response at all three chordwise locations, and the predictions agree well with the data. Figure 15 shows the suction-side waveforms for this radial station. Here, the experimental data show a highly nonlinear response across the blade chord at all three chordwise locations: x/c = 0.299, 0.565, and 0.698. Since the nonlinear response occurs over the entire chord, it may not be due only to the leading edge vortex. The waveform's double hump may indicate the formation and the convection and/or breakdown of a separation bubble (spanning the blade chord ?) twice during a revolution – once during the upstroke (the large hump) and once during the downstroke (the small hump). The 9-ft-diameter propeller rotates at 1671 rpm, and the rotational velocity at the 90-percent radius is four times the axial velocity. The time per revolution is an order of magnitude higher than the time required for a disturbance to traverse the chord. This may partly explain the nearly inphase nature of the measured waveforms at the three chordwise locations. It is not clear if the phenomenon is related to the dynamic stall of an oscillating thin airfoil where a small change in incidence angle produces a significant change over most of the chord (ref. 15). The present analysis does not capture the complex nonlinear response, which seems to result from unsteady viscous flow separation phenomena. Perhaps, a Navier-Stokes analysis accounting for viscous and turbulence effects may be able to simulate such nonlinear pressure responses.

Concluding Remarks

Numerical solutions of the unsteady, three-dimensional Euler equations were obtained for angular flow through a propeller for Mach numbers 0.5 and 0.2. For an inflow Mach number of 0.5, the phase of the predicted pressure response agrees well with measurements, whereas the magnitudes are underpredicted. At takeoff conditions (Mach 0.2) with high loading (blade setting angle at 75-percent radius is 31.6°), the prediction shows the formation of a leading edge vortex, which is in qualitative agreement with the data. However, the highly nonlinear response measured over the entire blade chord on the suction surface at this Mach number is not predicted by the present inviscid analysis. Accounting for the viscous and turbulence effects with appropriate resolution of the length and time scales may shed light on the highly nonlinear measured response.

References

1. Bushnell, P.: Measurement of the Steady Surface Pressure Distribution on a Single Rotation Large-Scale Advanced Propfan Blade at Mach Numbers from 0.03 to 0.78. NASA CR-182124, 1988.

2. Bushnell, P.; Gruber, M.; and Parzych, D.: Measurement of Unsteady Blade Surface Pressure on a Single Rotation Large-Scale Advanced Propfan With Angular and Wake Inflow at Mach Numbers from 0.02 to 0.70. NASA CR-182123, 1988.

3. Nallasamy, M.; Yamamoto, O.; Warsi, S., and Bober, L.J.: Large-Scale Advanced Propeller Blade Pressure Distributions: Prediction and Data, AIAA Paper 89-2696, July 1989 (Also, NASA TM-102316).

4. Whitfield, D.L.; Swafford, T.W.; Janus, J.M.; Mulac, R.A.; and Belk, D.M.: Three Dimensional Unsteady Euler Solutions for Propfans and Counter-Rotating Propfans in Transonic Flow. AIAA Paper 87-1197, June 1987.

5. Janus, J.M.; and Whitfield, D.L.: A Simple Time Accurate Turbomachinery Algorithm With Numerical Solutions of an Uneven Blade Count Configuration. AIAA Paper 89-0206, Jan. 1989.

6. Nallasamy, M.; and Groeneweg, J.F.: Prediction of Unsteady Blade Surface Pressures on an Advanced Propeller at an Angle of Attack. AIAA Paper 89-1060, Apr. 1989.

7. Nallasamy, M.; and Groeneweg, J.F.: Unsteady Euler Analysis of the Flow Field of a Propfan at an Angle of Attack. AIAA Paper 90-0339, Jan. 1990 (Also, NASA TM-102426).

8. Warsi, S.A.: User's Guide to PMESH: A Grid-Generation Program for Single-Rotation and Counterrotation Advanced Turboprops. NASA CR-185156, 1989.

9. Vaczy, C.M.; and McCormick, D.C.: A Study of the Leading Edge Vortex and Tip Vortex on Prop-Fan Blades. J. Turbomachinery, Vol. 109, No. 3, July 1987, pp. 325-333.

10. Stefko, G.L.; Rose, G.E.; and Podboy, G.G.: Wind Tunnel Performance Results of an Aeroelastically Scaled 2/9 Model of the PTA Flight Test Propfan. AIAA Paper 87-1893, June 1987 (Also, NASA TM-89917).

11. Rizzetta, D.P.; and Shang, J.S.: Numerical Simulation of Leading Edge Vortex Flows. AIAA Journal, Vol. 24, No. 2, Feb. 1986, pp. 237-245.

12. Rizzi, A.W.; and Eriksson, L.E.: Computation of Flow Around Wings Based on the Euler Equations, Journal of Fluid Mechanics, Vol. 148, Nov. 1984, pp. 45-71.

13. Smith, J.H.B.: Vortex Flows in Aerodynamics. Annual Review of Fluid Mechanics, vol. 18, M. Van Dyke, J.V. Wehausen, and J.L. Lumley, eds., Annual Reviews Inc., Palo Alto, CA, 1986, pp. 221-242.

14. Kandil, O.A.; and Chuang, A.H.: Influence of Numerical Dissipation on Computational Euler Equations for Vortex Dominated Flows. AIAA Journal, Vol. 25, No. 11, Nov. 1987, pp. 1426-1434.

15. Reddy, T.S.R.; and Kaza, K.R.V.: A Comparative Study of Some Dynamic Stall Models. NASA TM-88917, 1987.
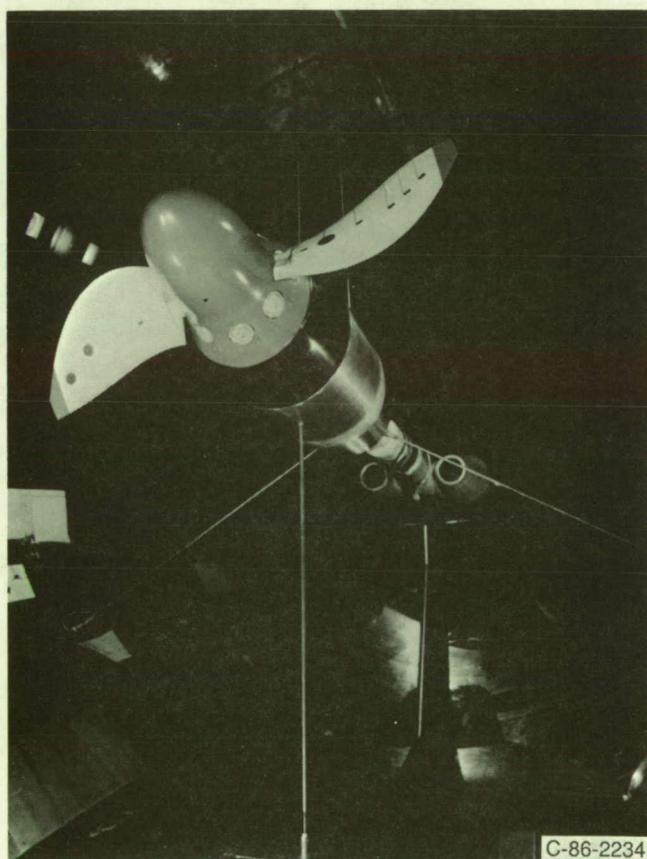
Figure 1.—SR7L propfan installed in the S1-MA transonic test section.

Outboard station, r/R = 0.91

Normalized
chord, x/c: .116   .279   .432   .565   .698   .898

Pressure tap: 19 18 1716 15 14

LE   TE

Pressure tap: 1 2 3 4 5 6
Pressure side

Suction side

x = 49.097 in.

Distance from hub,
x = 48.440 in.

Leading edge (LE)

x = 35.585 in.

x = 34.412 in.

Inboard station, r/R = 0.64

Normalized
chord, x/c: .049 .100 .233 .367 .500 .633   .833

Pressure tap: 26 25   24   23   22   21   20

LE   TE

Pressure tap: 7 8   9   10   11   12   13
Pressure side

Suction side

Trailing
edge
(TE)
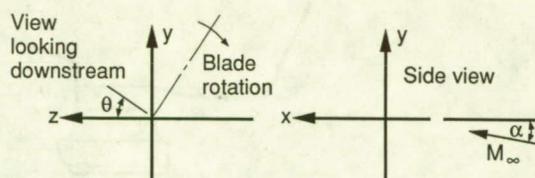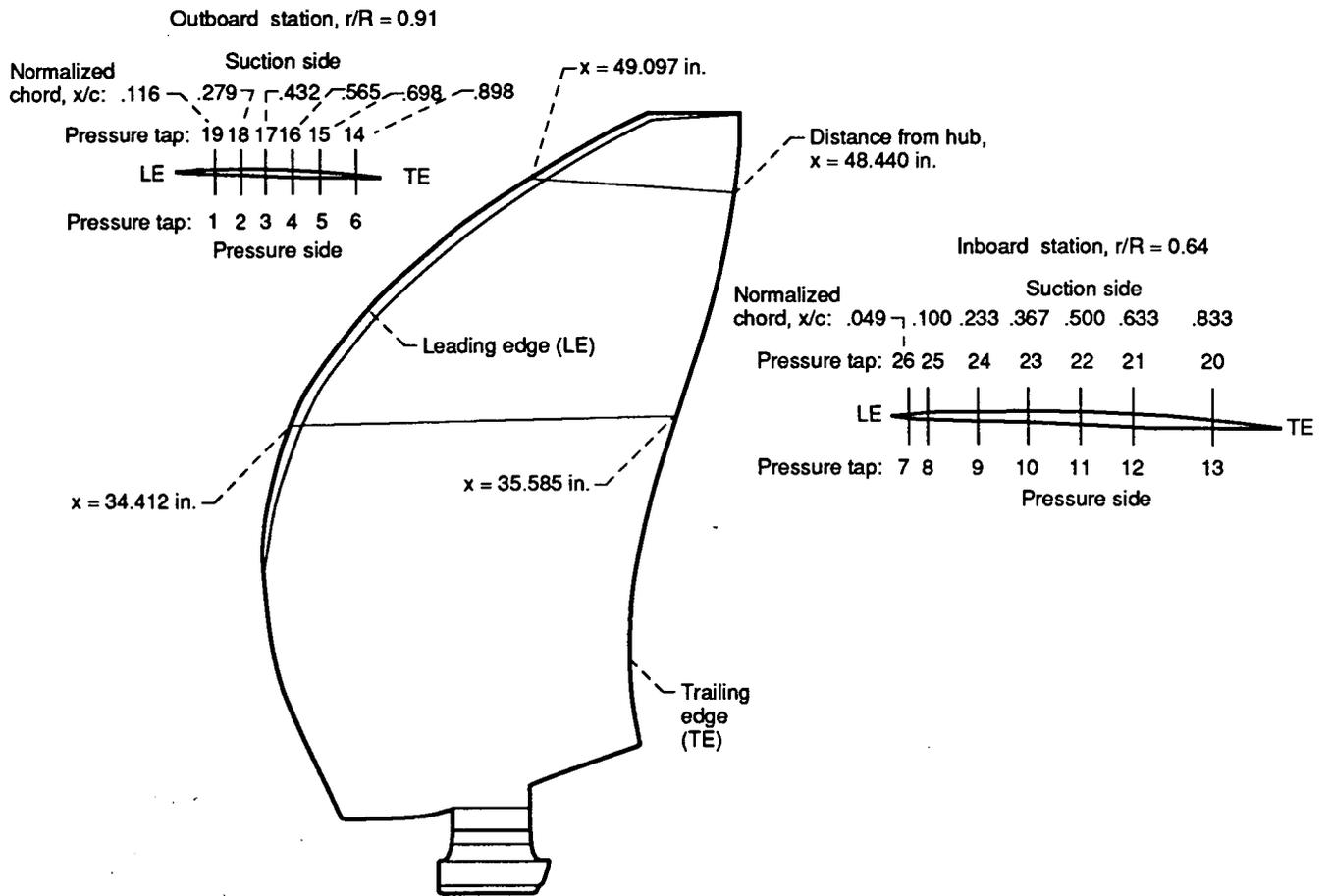
Figure 2.—Transducer locations for unsteady pressure measurements.
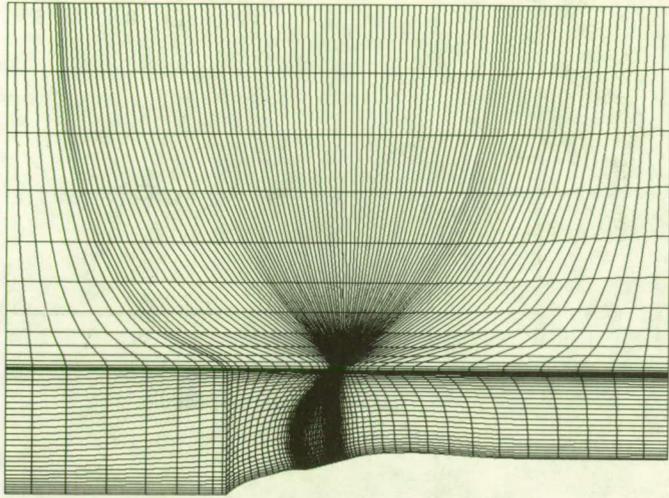
(a) Bladewise surface.
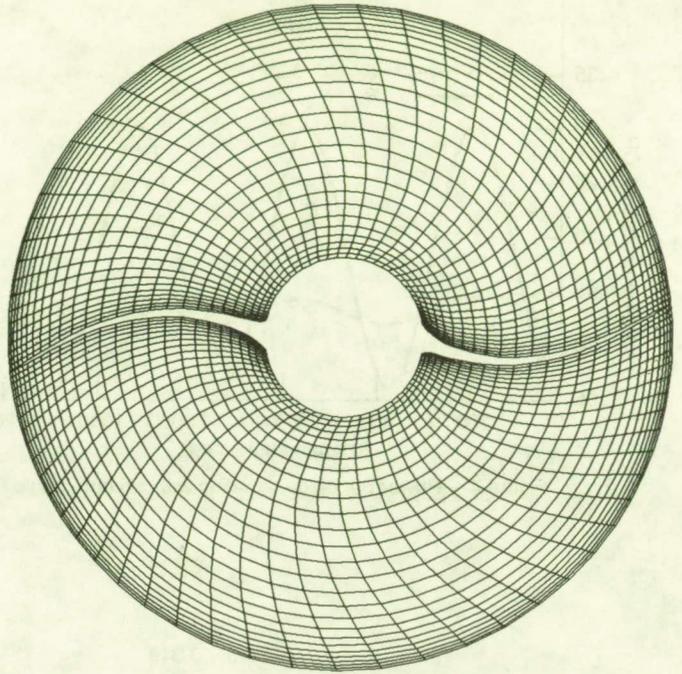
(c) Spanwise surface.
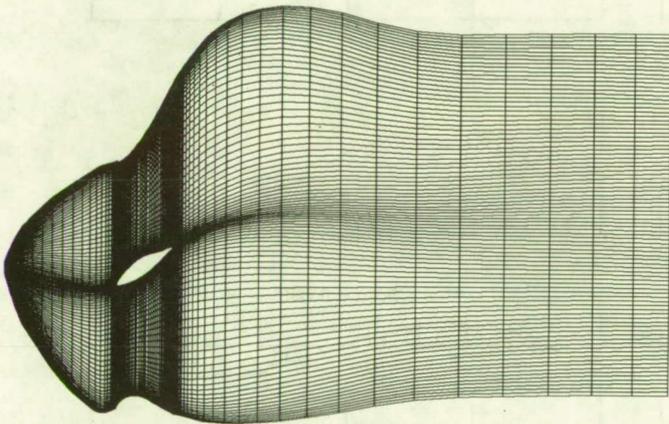
(b) Streamwise surface.
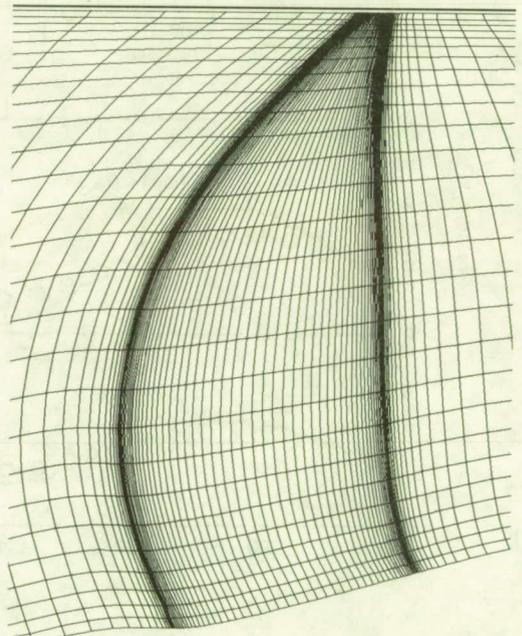
(d) Distribution of grid points on and near the blade surface.

Figure 3.—Typical computational grid.

7
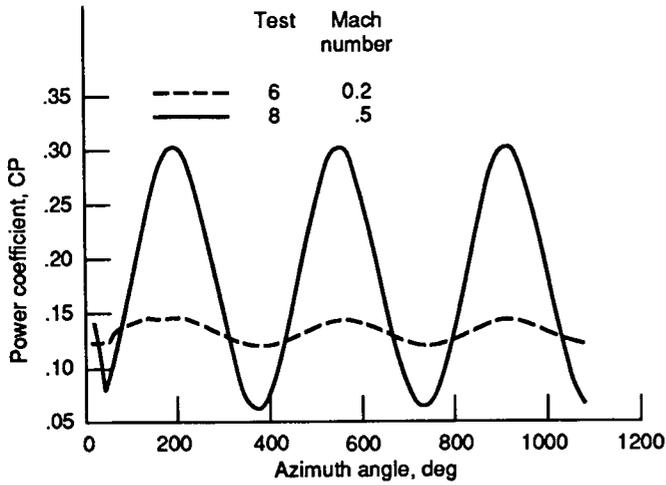
Figure 4.—Power per blade variation with azimuth angle.
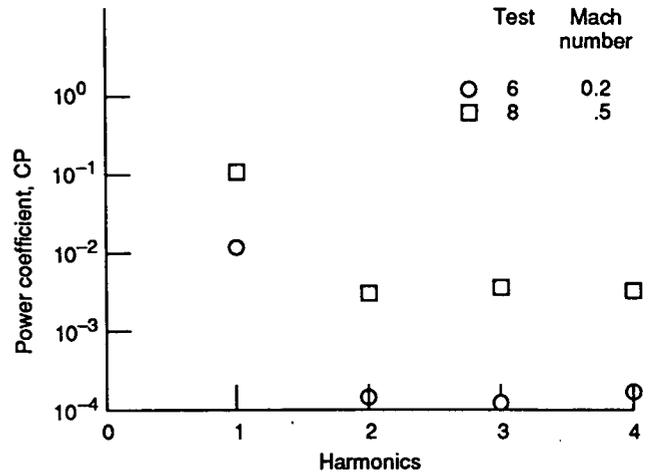
Figure 5.—Loading spectrum.

Chord = 0.049

Chord = 0.1

—— Data
O Prediction

Chord = 0.233

Chord = 0.367

Chord = 0.5

Chord = 0.633

Chord = 0.833
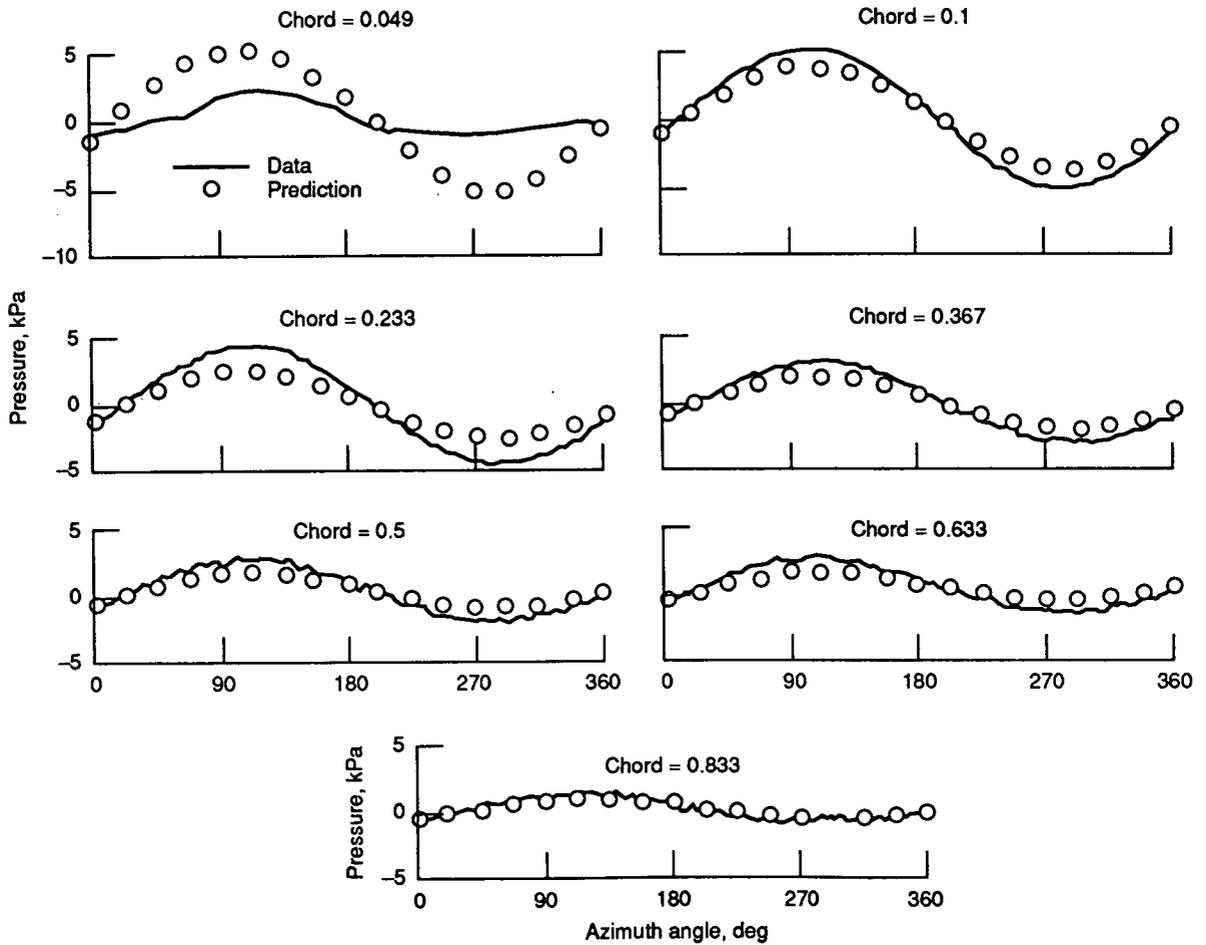
Figure 6.—Azimuthal variation of blade surface pressure on the pressure surface at radius ratio, r/R, 0.641. Test 8; Mach 0.5; advance ratio, J, 3.062.

8
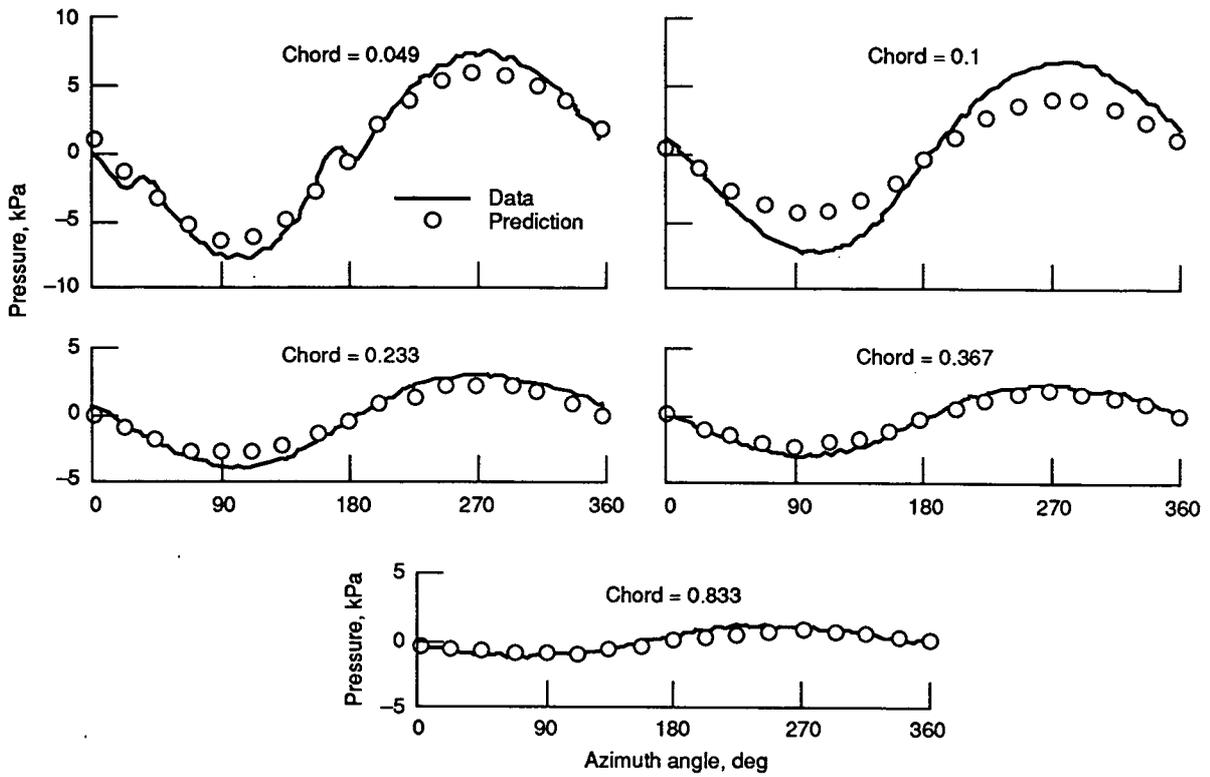
Figure 7.—Azimuthal variation of blade surface pressure on the suction surface at radius ratio, r/R, 0.641. Test 8; Mach 0.5; advance ratio, J, 3.062.
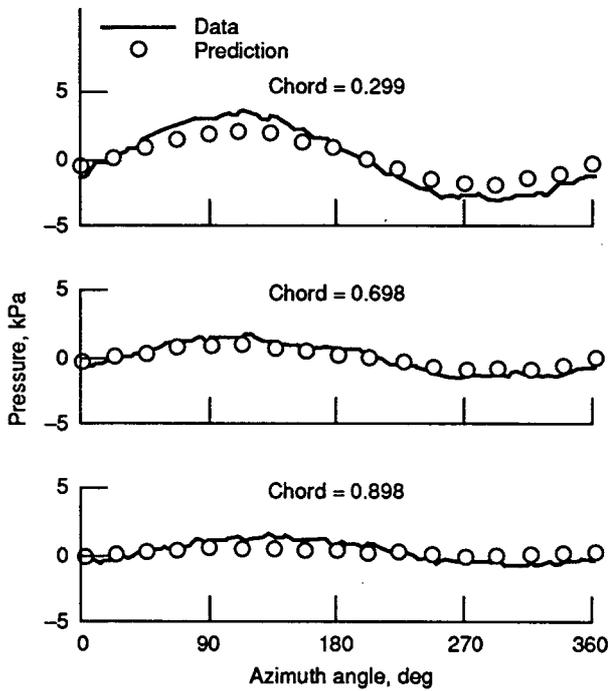
Figure 8.—Azimuthal variation of blade surface pressure on the pressure surface at radius ratio, r/R, 0.906. Test 8; Mach 0.5; advance ratio, J, 3.062.
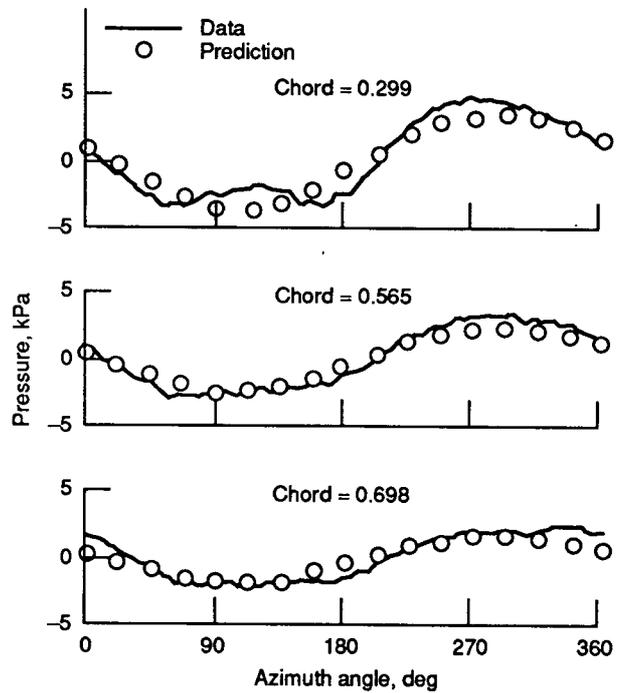
Figure 9.—Azimuthal variation of blade surface pressure on the suction surface at radius ratio, r/R, 0.906. Test 8; Mach 0.5; advance ratio, J, 3.062.

9
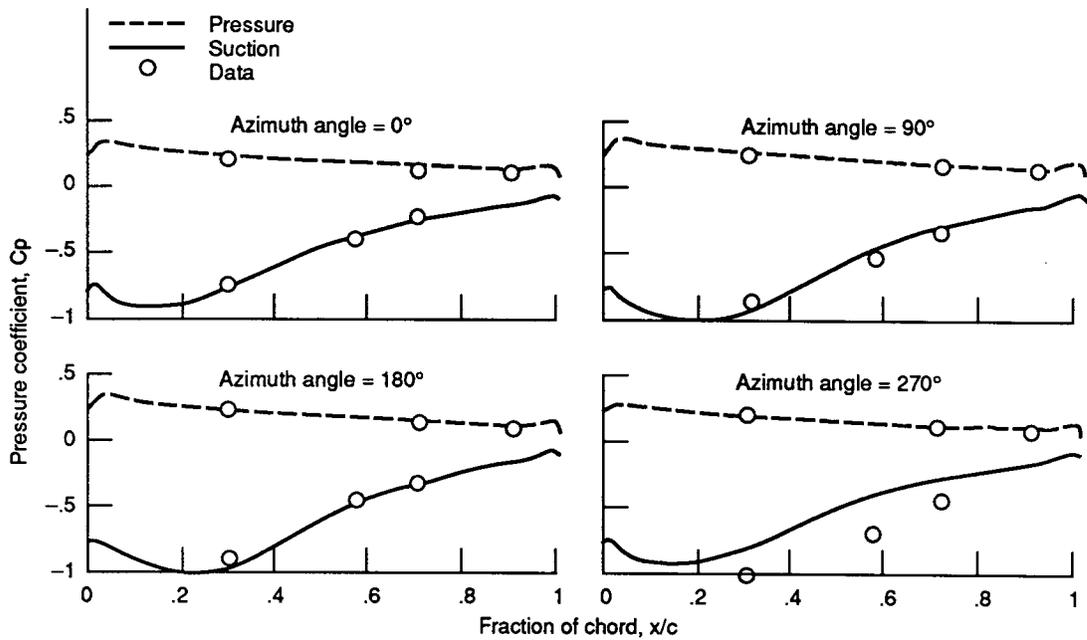
Figure 10.—Predicted and measured azimuthal variation of chordwise pressure coefficient at radius ratio, r/R, 0.9. Test 6; Mach 0.2; advance ratio, J, 0.881.

Static
pressure,

.75
.70
.65
.60
.55
.50
.45
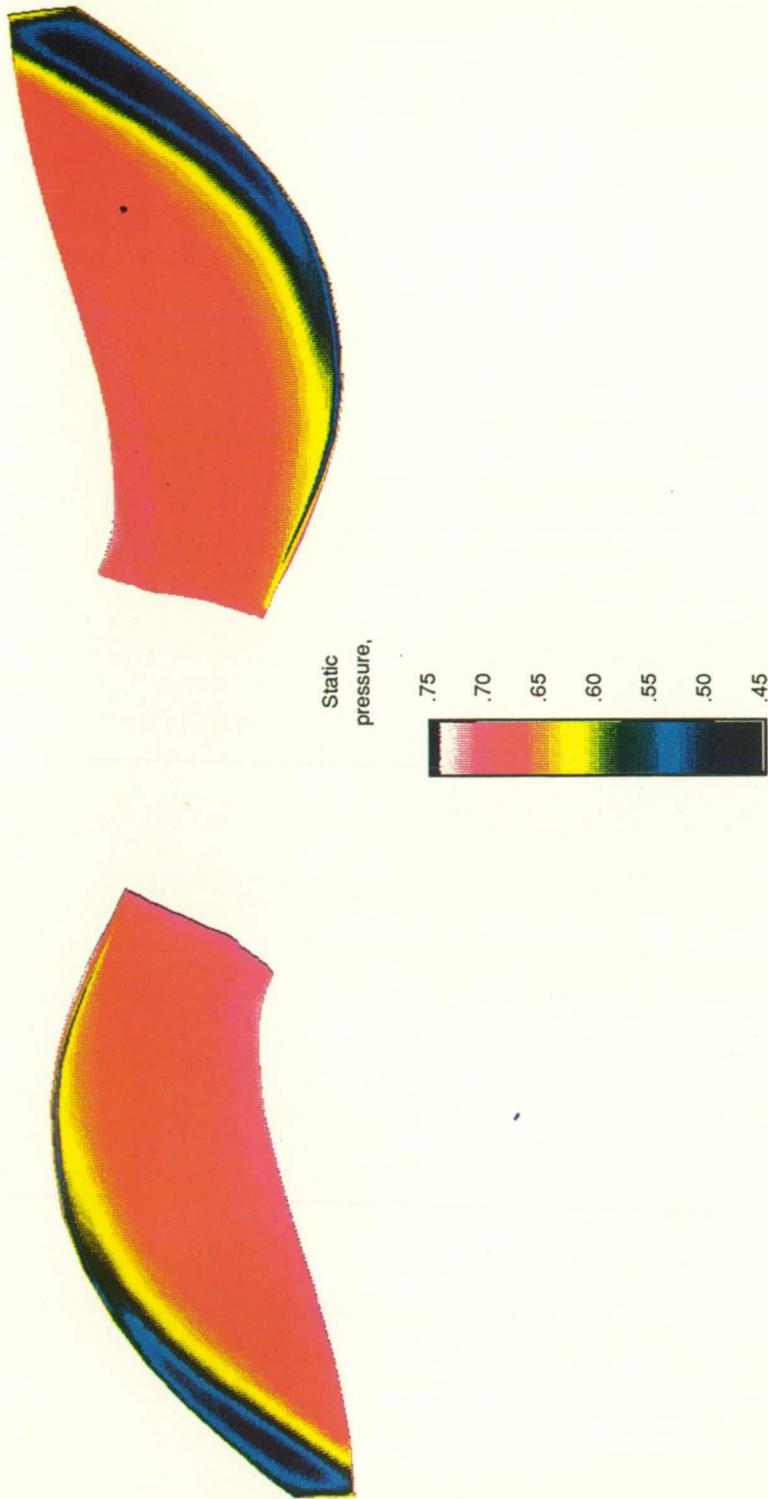
Figure 11.—Static pressure contours on the suction surfaces of the upward-moving and downward-moving blades: low-pressure region indicates the leading-edge vortex. Test 6; Mach 0.2; inflow angle, 3°.

11
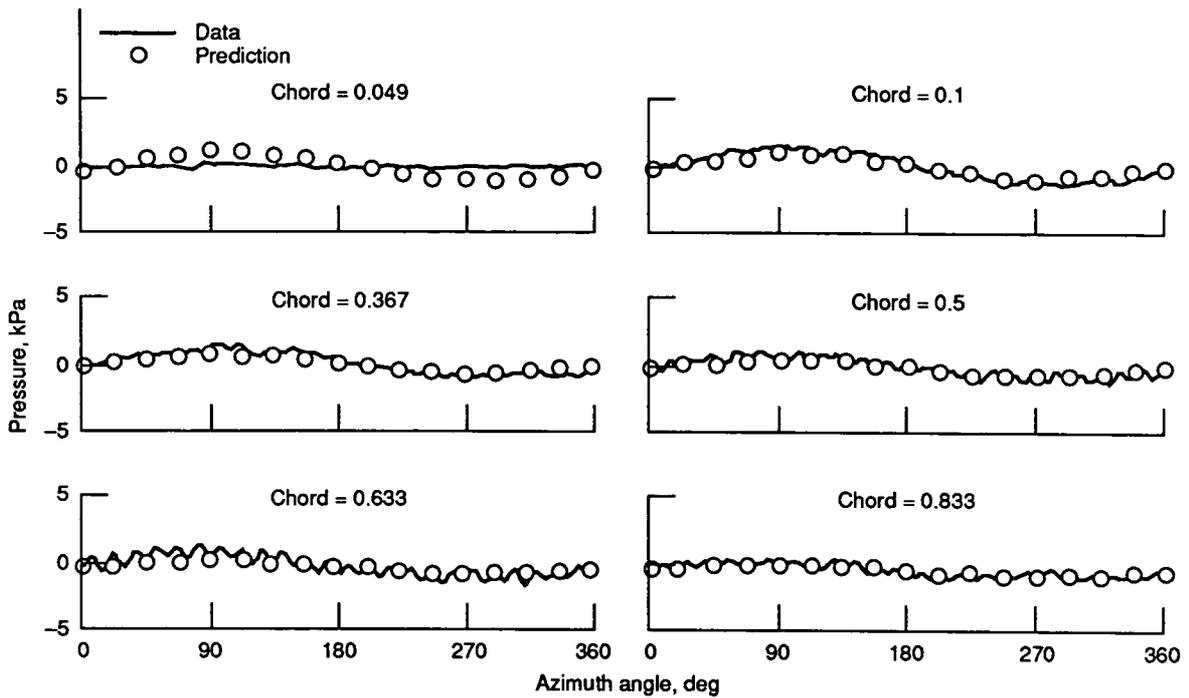
Figure 12.—Azimuthal variation of blade surface pressure on the pressure surface at radius ratio, r/R, 0.641. Test 6; Mach 0.2; advance ratio, J, 0.881.
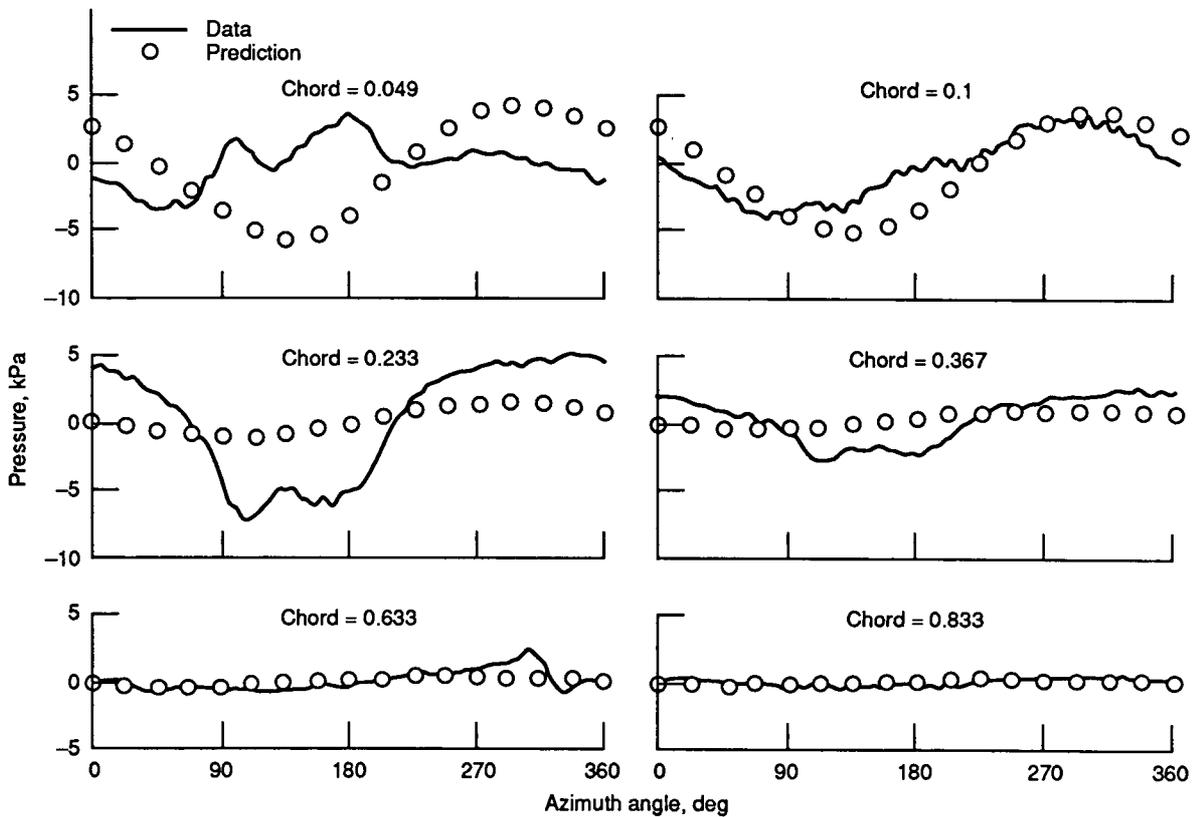

Figure 13.—Azimuthal variation of blade surface pressure on the suction surface at radius ratio, r/R, 0.641. Test 6; Mach 0.2; advance ratio, J, 0.881.

13
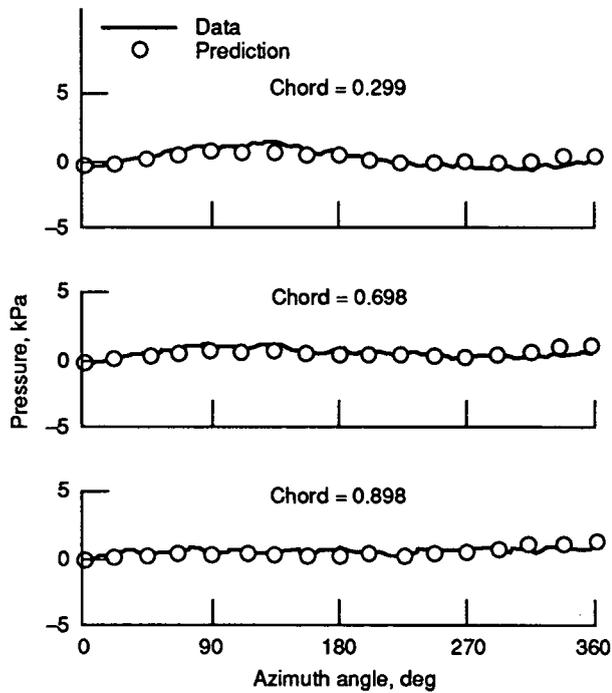
Figure 14.—Azimuthal variation of blade surface pressure on the pressure surface at radius ratio, r/R, 0.906. Test 6; Mach 0.2; advance ratio, J, 0.881.
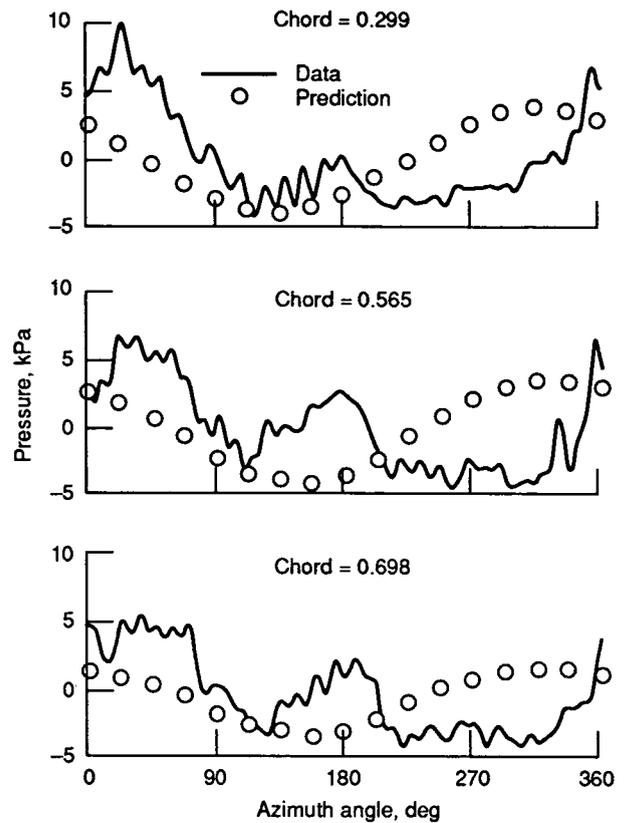
Figure 15.—Azimuthal variation of blade surface pressure on the suction surface at radius ratio, r/R, 0.906. Test 6; Mach 0.2; advance ratio, J, 0.881.

1. Report No. NASA TM-103218	2. Government Accession No.	3. Recipient's Catalog No.
4. Title and Subtitle Unsteady Blade-Surface Pressures on a Large-Scale Advanced Propeller: Prediction and Data		5. Report Date
		6. Performing Organization Code
7. Author(s) M. Nallasamy and J.F. Groeneweg		8. Performing Organization Report No. E-5630
		10. Work Unit No. 505-62-4D
9. Performing Organization Name and Address National Aeronautics and Space Administration Lewis Research Center Cleveland, Ohio 44135-3191		11. Contract or Grant No.
		13. Type of Report and Period Covered Technical Memorandum
12. Sponsoring Agency Name and Address National Aeronautics and Space Administration Washington, D.C. 20546-0001		14. Sponsoring Agency Code

16. Abstract

An unsteady, three-dimensional Euler analysis technique was used to compute the flowfield of an advanced propeller operating at an angle of attack. The predicted blade pressure waveforms for an angular inflow of 3° were compared with wind tunnel data at two Mach numbers, 0.5 and 0.2. For an inflow Mach number of 0.5, the predicted pressure response is in fair agreement with data: the predicted phases of the waveforms are in close agreement with data, whereas the magnitudes are underpredicted. At the low Mach number of 0.2 (takeoff), the numerical solution shows the formation of a leading-edge vortex, which is in qualitative agreement with measurements. However, the highly nonlinear pressure response measured on the blade suction surface is not captured in the present inviscid analysis.

17. Key Words (Suggested by Author(s)) Turboprops Unsteady Euler solutions Unsteady pressures Acoustics	18. Distribution Statement Unclassified – Unlimited Subject Category 71

19. Security Classif. (of this report) Unclassified	20. Security Classif. (of this page) Unclassified	21. No. of pages 16	22. Price* A02

National Aeronautics and
Space Administration

Lewis Research Center
Cleveland, Ohio 44135

FOURTH CLASS MAIL

ADDRESS CORRECTION REQUESTED

U.S.MAIL

NASA